IEEE Open Journal of
Antennas and Propagation

Received 14 December 2022; revised 11 January 2023; accepted 13 January 2023. Date of publication 24 January 2023; date of current version 21 February 2023.

Digital Object Identifier 10.1109/OJAP.2023.3239369

Wearable Antennas for Virtual Reality Cross-Body Links

WENJING SU (Member, IEEE), PRATHAP VALALE PRASANNAKUMAR (Member, IEEE), YIXIANG LI, GENG YE, AND JIANG ZHU (Fellow, IEEE)

(Invited Paper)

Reality Labs, Meta Platforms Inc., Menlo Park, CA 94025, USA

CORRESPONDING AUTHORS: W. SU AND J. ZHU (e-mail: wenjingsu@meta.com; jiangzhu@ieee.com)

This work was supported by Meta Platforms Inc.

ABSTRACT Cross-body link refers to the wireless connection between two wearable devices when they are both worn or near the body, such as that of a virtual reality (VR) headset and its controllers. It is one of the most challenging wireless scenarios in terms of link budget, due to severe shadowing effects when controllers are placed at the back side of the body. This is especially true when the users are in an outdoor environment where there is less reflection from the surrounding. This paper investigates the wireless propagation mechanism, including line-of-sight, ground reflection, and creeping waves. Based on that, through simulation and measurement experiments, this work analyzes the impact of different antenna designs on the cross-body link of VR/AR devices, including one novel compact low-profile antenna named Distributed Monopole (DM), and two conventional antennas. Due to the polarization advantages, both the novel DM antenna and the patch antenna shows significantly better performance than the dipole antenna. The DM antenna also shows a 2-4 dB advantage over the patch antenna due to its omni-directional field pattern. Time-domain analysis and statistical approaches are suggested to fully characterize the cross-body link of VR/AR antennas and body propagation.

INDEX TERMS Wearable antenna, body area network (BAN), ultrawide band (UWB), shadowing effect, creeping wave, ground reflection.

I. INTRODUCTION

IMMERSIVE computing has the promise to become the next major mobile computing platform. In the recent years, virtual reality (VR) and augmented reality (AR) are gradually walking out from the fiction movies and coming to everyone's life. More natural interaction experiences and new VR/AR applications attract increasing attentions, and the VR/AR industry has grown tremendously in the past years [1]. Owing to the on-body sensors and powerful on-head display, playing 3D games, dancing with friends in different countries, and working out with a virtual coach become everyday life of many people. However, with the growth in system complexity and high-throughput, low-latency requirement for 3D immersive experiences, a robust communication link between the input devices and output device becomes more important than ever. Any disconnection can directly lead to a disruption that negatively impacts the user experience.

VR/AR architecture often contains an output component on the head (e.g., head-mount display (HMD)) and input components on the hand (e.g., controllers on hands or other on-body sensors). With such architecture, the wireless link between hand and head is critical to be both low-latency to realize real-time feedback and high data rate to empower all the sensing capabilities. In the meanwhile, human body has a high dielectric constant and finite conductivity [2]. Designing antennas against human body is always challenging due to body effects, including de-tuning effects, attenuation effects, and shadowing effects. The shadowing effect is the most concerning for the cross-body communication and it is especially

severe in the low-reflection environments (e.g., outdoor). Prior works on body-centric communication and wearable antenna design lay a great foundation to this work [3], [4], [5], [6], [7], [8], yet none of them focuses on the immersive wearable computing applications and challenges. This paper aims to address how to design antennas to maintain a robust cross-body link with the shadowing effect from the human body taken into account. Different phenomena are discussed and tested to provide an optimal solution to the cross-body link puzzle. 8GHz which enables ultra-wideband (UWB) technology are used in this work as an example, since cross-body issue is especially challenging at higher frequencies. However, similar methodology can be scaled down to Wi-Fi and Bluetooth frequencies easily.

This paper discusses the VR/AR antenna design challenges, especially for cross-body link, and arranges in such way: Section II discusses the special problem from the point-to-point communication for on-body system, following by an in-depth analysis of cross-body link and propagation mechanism such as shadowing effect, reflection, and creeping wave. Section III focuses on the VR cross-body antenna design, including different antenna design considerations such as polarization and radiation direction. Based on the creeping wave theory, a novel compact UWB antenna is proposed and compared with different conventional antennas in Section III.

II. CROSS-BODY LINK

A. ON-BODY POINT-TO-POINT COMMUNICATION

In the VR/AR system, there are two kinds of communication links: on-body link and off-body link. The off-body link antenna design and evaluation process can be similar to the traditional consumer hardware antenna, such as antennas on cell phones or tablet. However, on-body antenna design can be quite different as its function focus on communication between two "fixed" points on body.

Talking about point-to-point communication, people often refer the Friis function, where antenna gain at the line-of-sight direction plays the biggest role and polarization of the two antennas need to be aligned. When calculating the link budget in the wireless system, similar methodology is adopted to calculating antenna gain and path loss. Even though the Friis Equation still gives us a good instinct of how a high gain antenna with the right beam direction and polarization can maximize the point-to-point link-budget, it is only working under assumption of far field and free space, which are both untrue for the on-body link. In this case, we cannot continue only considering the line-of-sight path. As demonstrated in Fig. 1, we call the link between two devices in the different side of the body as a cross-body link. While the TX and RX can be anywhere, we have TX on the head and RX on the back as an example to represent the case of VR headset to hand-hold controller link when the hand is on the back during the dancing or gaming activities. From the Fig. 1, there is clearly three possible paths between the TX and RX: 1. Line-of-sight (LoS) 2. Ground reflection 3. Creeping wave. The next three subsections will discuss them one by one.

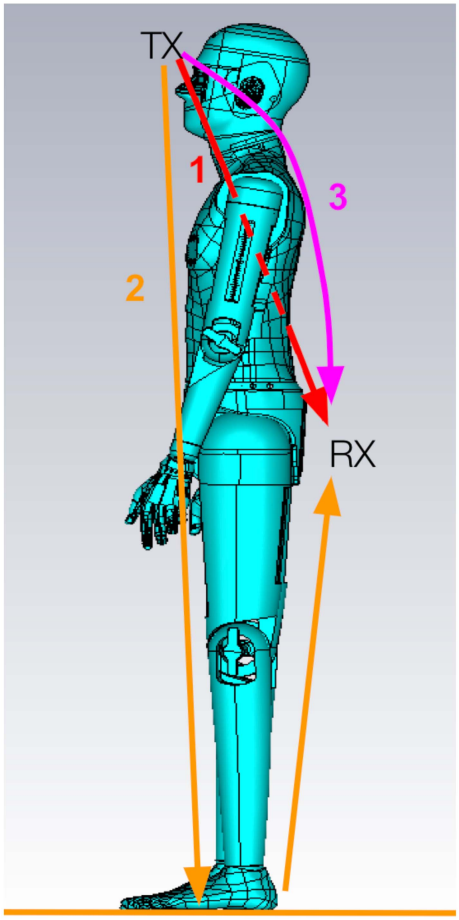

FIGURE 1. A picture of potential cross-body link path from forehead to back of the body. 1 represents the light-of-sight, 2 refers to ground reflection, and 3 shows one possible creeping wave path. An SPEAG POPEYE10 phantom model is used to represent the human body.

Besides the path uncertainty, another complexity is due to the fact that humans are alive. This means the on-body Point-to-Point link can vary a lot with different person, in different environments, at different time [10], [11]. It is easy to imagine that user moves their hands around the body while using the VR/AR devices which can result in the link loss changing dramatically during the activities. The good news is that to optimize the link, it's not necessary to improve all the case but majorly the worst case where the link breaks. However, even if we focus on the worst location, such as VR headset to controller on the back of the body, there are still many variation factors. Table 1 shows the different tissue properties at frequencies of Bluetooth (BT), Bluetooth Low Energy (BLE), Wi-Fi, and Ultra-wide Band (UWB), which are common connectivity technologies in consumer hardware for on-body link. It is easy to see in Table 1 that higher frequencies the permittivity decreases slightly but the conductivity increases dramatically. Comparing to Wi-Fi or Bluetooth at lower frequencies, cross-body link is especially

TABLE 1. Dielectric properties of body tissues [2], [9].

Frequency	2.4 GHz		5 GHz		8 GHz	
Tissue	E_r	σ(S/m)	E_r	σ(S/m)	E_r	σ(S/m)
Skin(dry)	38.1	1.44	35.8	3.06	33.2	5.82
Skin(Wet)	42.9	1.56	39.6	3.57	35.9	6.68
Muscle	53.6	1.77	49.5	4.04	45.5	7.80
Fat	5.29	0.102	5.03	0.242	4.76	0.443

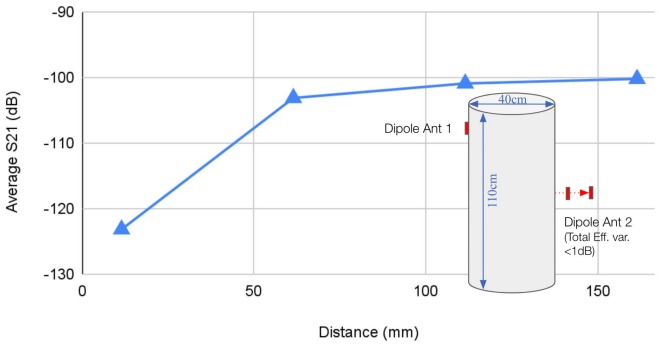

FIGURE 2. Simulation results of average S21 in the UWB channel 9 with different distance from Dipole antenna 2 to the cylinder with an inserted picture demonstrate the simulation setup.

challenging for UWB in consumer hardware, because of both higher pathloss and higher body conductivity. Table 1 also shows the skin conductivity can be quickly changed for the same person before and after working-out due to sweat, and person with a different body fat/muscle percentage have a quite different body property even if they happen to have the same shape of the body.

B. LINE-OF-SIGHT

The red path in the Fig. 1 represents the line-of-sight link. The permittivity and conductivity in Table 1 indicate that penetrating through the body is challenging. This phenomenon that line-of-sight link being blocked by the human body usually refers as shadowing effect, which instinctively reminds people of light shadows. In the VR case, it can be imagined as user wearing a head light with the shadow on the back. There are also studies on the communication perspective to characterize such kind of shadowing effect [3], [10]. To obtain a straight-forward view of the shadowing effect, an experiment is designed in the CST microwave studio simulation with one cylinder with body material representing human and two simple dipole antennas, as shown in Fig. 2. The antenna 1 is near the edge of the cylinder, and the antenna 2 is on the opposite side near the middle of the cylinder. The numerical average S21 in the UWB channel 9 frequencies (7.75GHz to 8.25GHz) is recorded while the distance between antenna 2 and the phantom is increased. To minimize the impact of detuning effect and attenuation effect, this study starts with 10 mm distance and 1.5mm substrate thickness (11.5 mm from dipole to body in total), so that the total efficiency changes is less than 1dB. Meanwhile,

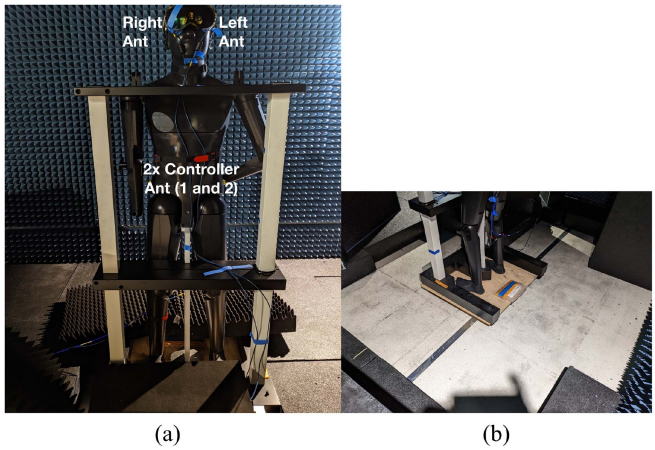

FIGURE 3. Measurement setup of (a) no ground reflection environment and (b) ground reflection environments.

the S21 increases from −123 dB to −100 dB with the distance increases. In this case, with the increasing distance d, the path loss is decreasing, which apparently doesn't follow the Friis function for LoS. This shows that LoS is no longer the dominant path for the signal between VR headset and controller in cross-body scenarios.

C. REFLECTION

When the LoS is blocked by the shadowing effect, the next to be considered is the reflection path. This is especially true for the indoor case. While the optimal reflection path in an indoor environment can be largely depends on the environment and user location, the rich reflection environments usually enable relatively robust links in the end with multiple potential reflection paths in different user activities [12]. On the other side, outdoor use cases with reflection only from the ground are more challenging and reasonable to study.

To better understand the ground reflection effect, a measurement setup in Fig. 3 is used. Two UWB antennas (left, right) are mounted inside of the left and right side of a Meta Quest Pro headset on the SPEAG POPEYE-10 phantom forehead and another two UWB antennas (ant 1, ant 2) are mounted inside the Meta Quest Pro controller in the phantom hand on the back. The insertion loss between the right headset antenna and ant 2 on the controller are defined as "right2," and likewise, there are right1, left1, and left2. Those S-parameters are recorded in Fig. 4 for both a no-ground-reflection case with absorbers covering the entire floor in Fig. 3(a), and a ground-reflection case with no absorber below the phantom area in Fig. 3(b). The test is done with an 4-port Vector Network Analyzer (VNA) in a anechoic chamber with all walls and ceiling covered by the absorbers. The measurement VNA as well as the tester are also well shield by the absorbers. Fig. 4 compares the S-parameters with and without the absorber on the ground, and shows a 4-8 dB boost in the peak S-parameter of right2 and left2 when the floor is exposed, which suggests that ground reflection can be

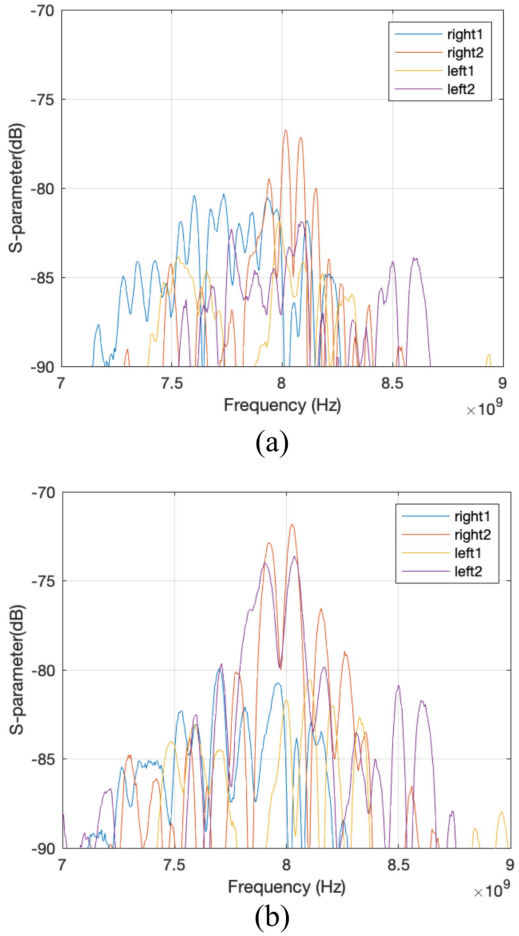

FIGURE 4. Measurement S-parameter (dB) of (a) no ground reflection environment and (b) ground reflection environments.

helpful to the cross-body link at the frequencies we are investigating. To further analyze where the boost, the S-parameter is being processed with Inverse fast Fourier transform (IFFT) in MATLAB to get the time domain response as showed in Fig. 5. The first pulse near 5 ns is marked in red and the rest are marked in blue. It's clear that the first pulse magnitude in (a) and (b) are the same as (c) and (d) respectively while the second pulses with a large magnitude near 12.5 ns in (c) and (d) are not existed in (a) and (b). The POPEYE phantom used in the test is 1.85 m tall and the shortest distance between HDM, floor, and controller is about 3 m which is in the similar range with the 12.5 ns pulse, indicating that the floor reflection path dominates in this link.

Even though significant improvements in the link strength can be found with ground reflection as discussed in the previous paragraph, more investigations are required to determine if ground reflection is the reliable path, for example, against different ground conditions and materials [13]. Further, in Fig. 4, unlike the left 2 link and the right 2 link, the left 1 link and the right 1 link show no obvious difference in the link strength between with and without absorber on the floor. This means the ground reflection is sensitive to the antenna location, orientation, and radiation pattern and the ground reflection path does not always help the link strength.

D. CREEPING WAVE

In the minimal reflection environments, such as anechoic chamber in Fig. 3(a), we can still see a strong link like the pulse at 5 ns in Fig. 5(a) and (b). This pulse is from the wave propagating around body surface, which has different names in different articles, such as creeping wave [3], [4], [10], [14], surface wave [5], body wave, ground wave, and Norton (surface) wave [5], [15]. Despite the different names, these all refers to a phenomenon similar to diffraction that wave propagate along the curved/bending surface of the lossy object/body. Creeping/surface wave can be a way to strongly boost the wireless communication [16] and comparing to reflection, it only depends on the human body surface thus can support robust link even in the worst environments.

III. CREEPING WAVE ANTENNAS

A. VR ANTENNA DESIGN

VR antenna design shares many requirements with the other consumer hardware, such as efficiency and bandwidth, but it has its own approach due to the special use case. Firstly, the ideal antenna for VR application should be efficient in radiation when mounted on head, while having uniform coverage around the user, that is, low antenna directivity. Besides that, the proximity of other sub-systems components, such as display, microphone, speakers, fans (with magnets), camera, and all the electrical flexible printed circuit board (PCBs) impacts the antenna's radiation efficiency and pattern. Moreover, the interaction between the antennas and the human head further challenges the design. Additionally, the weight and cost constraints of the product govern the type and size of VR antennas.

B. DISTRIBUTED MONOPOLE ANTENNA

Monopole and dipole antenna polarized perpendicular to the skin have been characterized as good candidates for exciting creeping waves from previous studies [15], [17], [18], [19]. However, those antennas inevitably are too tall for the practice use in the compact and low-profile consumer electronic devices and thus not fit the above-described VR antenna consideration. Moreover, the difference in antenna heights makes it questionable to directly compare the cross-body link performance with respective to antenna's polarization. To this end, a new antenna, namely *distributed monopole (DM) antenna* has been proposed in this paper as show in the Fig. 6(a) and (b). The DM antenna has similar properties of monopole antenna but has a compact size and a very low profile. As shown in Fig. 7, the DM antenna has a free space radiation pattern similar to monopole and is rotational symmetrical as monopole. A DM antenna has been designed to operate at UWB Channel 9. DM antenna has a size of 8.6 mm by 8.6 mm which is comparable to 9 mm by

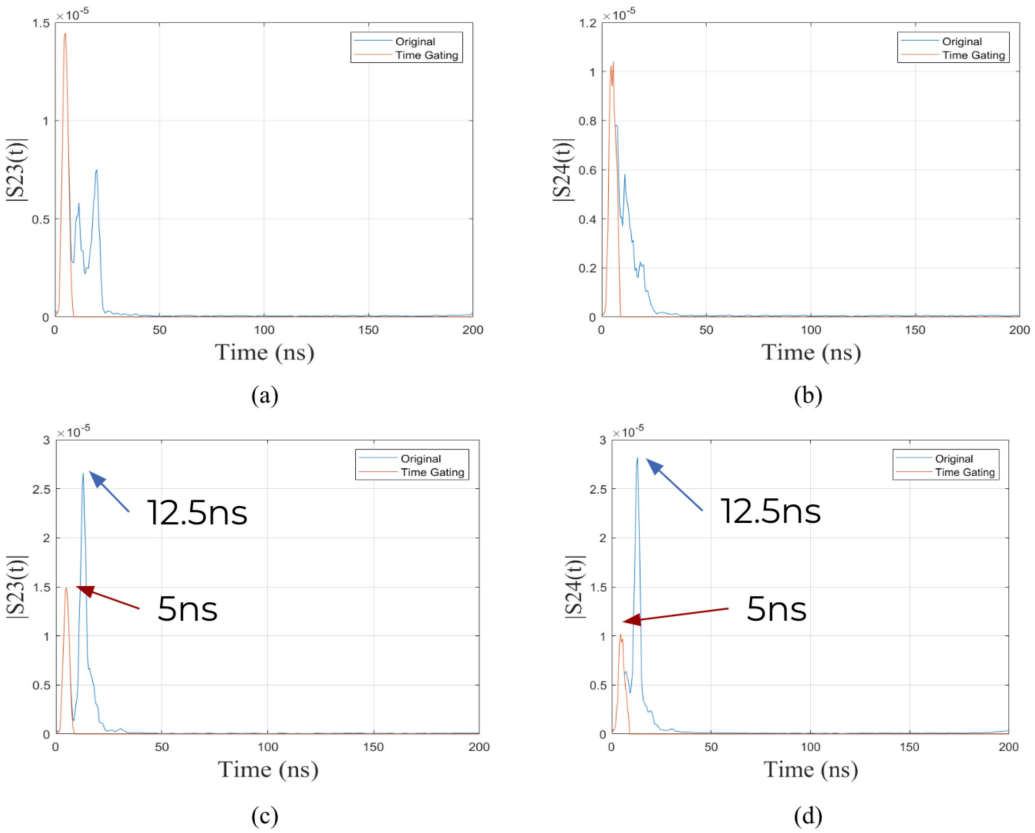

FIGURE 5. IFFT of S-parameter (dB) of (a) right-2 link and (b)left-2 link in no ground reflection environment and (c) right-2 link and (d)left-2 link in ground reflection environments. The red curves show time-gating of the first 7.5 ns and blue curves show the rest.

9 mm size of patch antenna working at the same frequencies as shown in Fig. 6(b) and (c). Each antenna has 13 mm by 13 mm ground plane and 1.5 mm thick substrate with Rogers RO4003C. The operation principle of the DM antenna is a negative permittivity material loaded zeroth-order resonance antenna [20]. The DM antenna consists of an array of cells that consist of pad and a shorting vias in the center. Each cell can be seen as a small monopole antenna and the array is excited by the feeding via. The specific design used in this paper is a cross shape with 5 cells, but it can be in different topologies, such as 5 cells in one row, and have different number of cells depending on the needs and available antenna volume. To work at 8GHz, each cell is made by 4.6 mm by 4.6 mm square with 0.2 mm vias in the center connected to the ground and cells are separated by 2mm to each other. DM, dipole, and patch antennas in this work feature a similar on-body antenna efficiency around −3.5dB for a fair comparison.

C. EXPERIMENT SETUPS AND METHODS

To compare different antennas, three experiments are done in simulation and/or measurements. The first experiment is shown in Fig. 8(a), where we have the similar setup as in Fig. 2: Cylinder represents “body”; antenna 1 is near one edge on top side to represent forehead; and antenna 2 is on the bottom side to represent hand on the back. In this simulation, 3 different antennas (DM antenna, patch antenna, and dipole antenna) with different orientations are moving along the bottom side of the cylinder. VV and HH means both antennas are in the vertical or horizontal orientations, while in both orientations the antennas are parallel to the cylinder surface. The average S21 in the UWB channel 9 is recorded in the Fig. 8(b).

The second experiment is done in both simulation and measurement. Instead of the cylinder in the previous experiment, an SPEAG POPEYE-10 phantom is used and five locations on the back are chosen as shown in the Fig. 9(a). The position 1 is the back right pocket location and position 2 are 10 cm higher in the center of the back. The position 3 and 5 are 20 cm directly higher or lower to position 2 and location 4 is directly 20 cm higher than position 1. The measured average S21 of each location for both DM antenna and Patch antenna are shown in Fig. 9(b). To better compare the antennas, the box chart of simulated and measured S21 are shown in Fig. 10.

The third experiment uses the setup in the Fig. 3(a) where two antennas (DM, patch, or dipole) are placed on the two sides of the Meta Quest Pro headset and

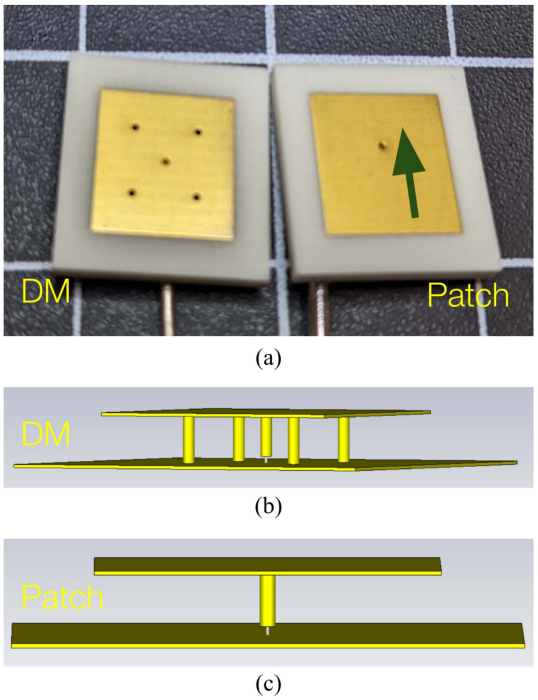

FIGURE 6. (a) Top view photo of DM antenna and Patch antenna side by side on a 0.5-inch pitch grid. The green arrow in the patch indicates the two radiation edge locations and was used to identify the patch orientation through the paper. (b) Side view of the DM antenna. (c) Side view of the patch antenna.

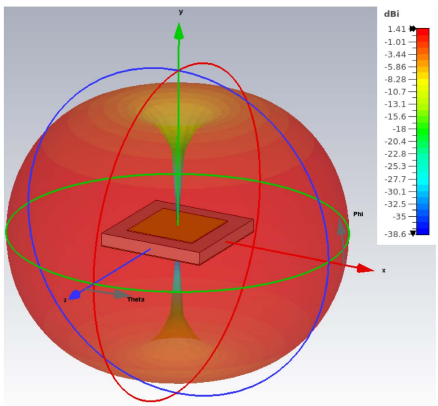

FIGURE 7. Free space radiation pattern of Distributed Monopole (DM) antenna at 8 GHz.

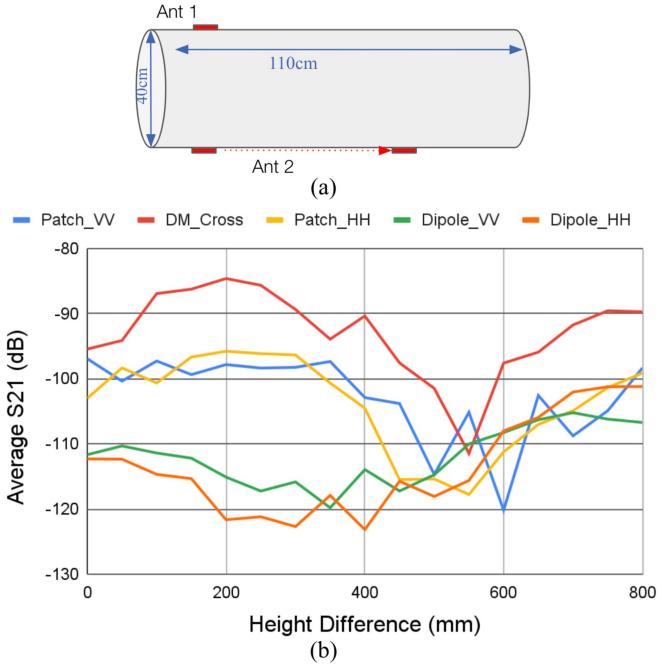

FIGURE 8. Experiment 1: (a) Simulation setup with a cylinder representing human body with two antennas on the opposite side and the second antenna move along the cylinder as arrow indicated. (b) Simulation results of average S21 in the UWB channel 9 with the setup demonstrated in (a).

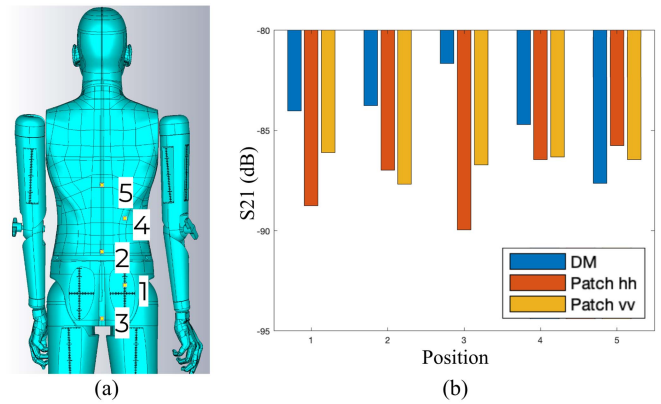

FIGURE 9. Experiment 2: (a) Antenna locations on the back (b) Measured S21 between the two antennas when back antenna in different locations.

two patch antennas are placed inside of controller with different orientations. Fig. 11 shows the example of measured S-parameters. The measured S-parameters are then post processed as such: assuming switch diversity of the two HMD antennas and two controller antennas, the best link of the four links between headset and controller is chosen and numerical averaged over the frequencies between 7.75 GHz and 8.25 GHz to represent the antenna performance. Seven different arm poses with different controller locations and orientations are used to cover different use cases and a cumulative distribution function (CDF) plot summarizes all the data collected in Fig. 12 for different antennas.

D. POLARIZATION

As discussed in [5], [15], [17], [18], [19], creeping wave is in favor of antenna that excite E-field that is perpendicular to the human body. Many of those studied uses dipole antenna with different orientation for the polarization comparison, however, the inherited height difference in different orientation might also play a role in the results as Fig. 2 already shows that 50 mm height difference can create 20dB difference. In our experiments, dipole antenna is placed parallel to the body surface which means that E-field is parallel to the body surface too, while DM antenna and patch antenna are placed at the same plane as the dipole antenna to provide a fair comparison. In experiment 1 in Fig. 8(b), dipole antenna in both orientations in general have a worse S21

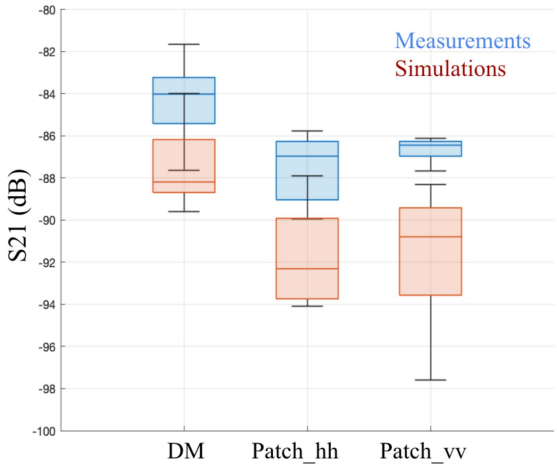

FIGURE 10. Experiment 2: Simulation and measurements results of different antenna link strength in a box chart.

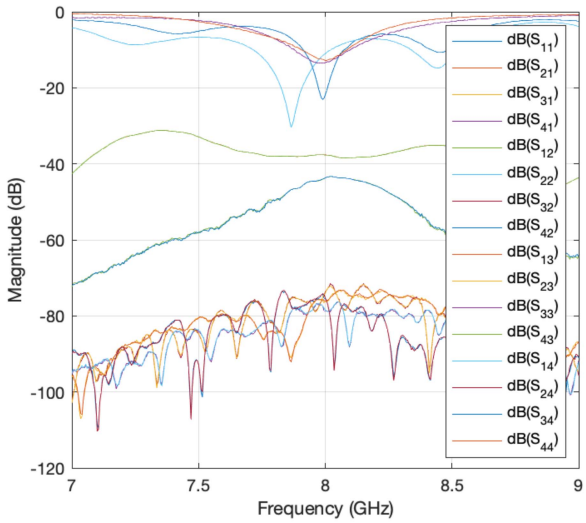

FIGURE 11. Experiment 3: Example of S-parameter measurement results in VNA.

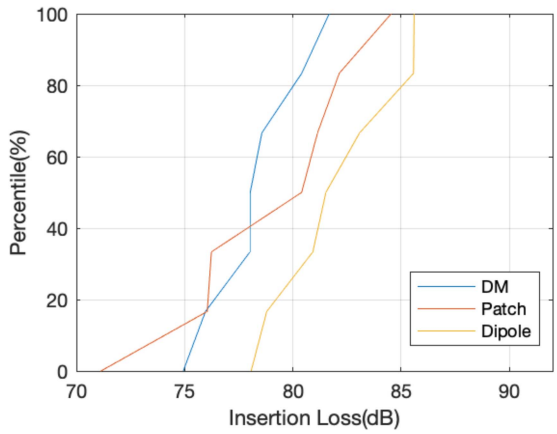

FIGURE 12. Experiment 3: CDF of the three antennas for VR cross-body link.

comparing to DM antenna and patch antenna with different orientations. For the full body phantom measurement (experiment 3) in Fig. 12, the dipole antenna also shows the worst link loss in the three antenna designs. These results

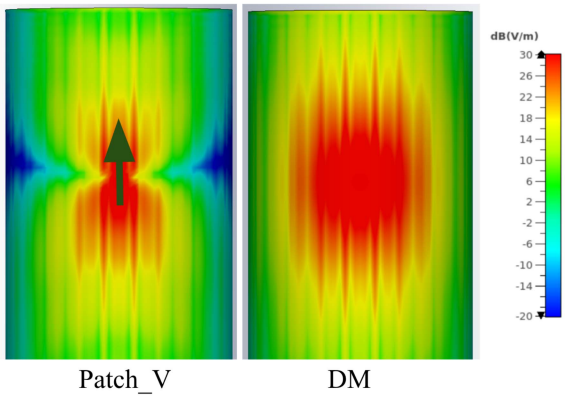

FIGURE 13. E-field maximum distribution of DM antenna and Patch antenna on top of a cylinder representing human body.

match well with the previous studies and the Norton surface wave theory [5]. Dipole antenna that is parallel to the body surface clearly shows worse performance than DM antenna and patch antenna that are also parallel to the body in all experiments.

E. RADIATION DIRECTION

While there are extensive studies on the impact of antenna polarization to body-centric propagation, the impact from antenna's radiation direction on the cross-body link are rarely investigated. Reference [17] points out the dipole with the same polarization can have a different link strength when placed in different orientation. The conclusion is obvious but also critical in the antenna design for VR/AR. This phenomenon can be observed in experiment 1 in Fig. 8(b) as well. When the same antennas are installed on top of a body cylinder and move along the back of the cylinder, different orientations can sometimes create more than 10 dB difference. Fig. 13 shows the E-field on the body cylinder in Fig. 8(a) for DM antenna and patch antenna which discloses part of the reason. The arrow direction in the patch matches the arrow in Fig. 6(a). It's clear that the field patterns of the two antennas are different. DM antenna, in this case, like a monopole antenna, has a more omni-directional radiation on the cylinder surface while the patch antenna radiation is directive to the two radiation edges. Given that both DM and patch features an E-field perpendicular to the body surface and are at the same height, the DM antenna shows 10dB better in many locations is likely due to its omni-directional radiation while patch antenna doesn't have a good coverage at those directions. Even though antenna far-field radiation can be easily represented by the radiation pattern and a gain value, but the radiation direction of creeping wave on the body surface is not necessarily correlate with the far-field pattern. Instead, the near-field pattern and E-field strength is the most relevant. This also matches the results in [15], where the E-field excited by different antenna degrades on the curve at the same rate that only related to the bending radius of the curve. In this case, an

antenna with field pattern or a great E-field strength ("gain") direct to the optimal path from head to hand on the back can have the best link performance.

F. MULTI-PATH

The body surface, unlike the cylinder in Fig. 13, is usually rather complex and the multi-path effect happens without an easy answer of optimal path. As discussed in [21], the major paths from one ear to another ear can be calculated with diffraction theory. However, with the complexity in different body shapes and activities, the constructive and destructive interference would change easily and make it almost impossible to identify the absolute path from head to hand. Therefore, statistic practice needs to be applied and a relative larger sample size is needed. In experiment 2, five positions on the back of the phantom are tested as shown in Fig. 9 (a) while Fig. 9 (b) are the measurement results with different antennas on those positions. The worst position of each antenna is different, and it is not necessarily to be the furthest position number 3. Same phenomena can be observed in Fig. 8(b) that every antenna has its own worst position when move along the back of the cylinder. In this case, one can never make any conclusion about different antenna designs with one measurement position. Fig. 10 shows the box chart of the simulated and measured results which is the statistic distribution of each antenna design. Even though the simulations and measurements still have few gaps, the overall trend is aligned. With a chart like such, it's easier to conclude that DM antenna is 2-4 dB better than the patch antenna in the cross-body head-to-hand cases. Similarly, in the experiment 3, when we embed those antennas into form factor and compare the DM antenna with the patch antenna, 2-4dB improvement in the median and worst cases are seen while patch antenna has a better the best case performance, likely due to the different antenna locations and the diversity architecture used in this test. The three experiments all show that the proposed DM antenna has a better radiation direction and a better coverage in the multi-path environments comparing to the patch antenna from a statistic point of view.

IV. CONCLUSION

This paper investigates the cross-body link for VR/AR antennas from existing challenges to potential solutions. Different path from head devices to hand devices are studied with simulations and measurements, including line-of-sight, ground reflection, and creeping wave. Two traditional antenna, patch antenna and dipole antenna, and one novel compact low-profile antenna, Distributed Monopole (DM), are used in the simulations and measurements to compare and understand what antenna would work best for the link, from different polarization, radiation directions, and multi-path effect on body. Across all the cross-body simulations and measurements, DM shows 2-4dB advantages over patch antenna due to its omni-directional field pattern, while dipole antenna shows the worst performance as its E-field polarization is parallel to the body surface. This work also demonstrates that time-domain analysis and statistic approaches are desired to fully characterize the cross-body link for VR/AR antenna and body propagation.

REFERENCES

[1] P. Rosedale, "Virtual reality: The next disruptor: A new kind of world-wide communication," *IEEE Consum. Electron. Mag.*, vol. 6, no. 1, pp. 48–50, Jan. 2017.

[2] FCC. "Body tissue dielectric parameters." Accessed: Oct. 10, 2022. [Online]. Available: https://www.fcc.gov/general/body-tissue-dielectric-parameters

[3] S. L. Cotton, "A statistical model for shadowed body-centric communications channels: Theory and validation," *IEEE Trans. Antennas Propag.*, vol. 62, no. 3, pp. 1416–1424, Mar. 2014.

[4] P. S. Hall and Y. Hao, "Antennas and propagation for body centric communications," in *Proc. 1st Eur. Conf. Antennas Propag.*, 2006, pp. 1–7.

[5] A. Lea, P. Hui, J. Ollikainen, and R. G. Vaughan, "Propagation between on-body antennas," *IEEE Trans. Antennas Propag.*, vol. 57, no. 11, pp. 3619–3627, Nov. 2009.

[6] M. Kim and J.-I. Takada, "Statistical model for 4.5-GHz narrowband on-body propagation channel with specific actions," *IEEE Antennas Wireless Propag. Lett.*, vol. 8, pp. 1250–1254, 2009.

[7] G. A. Conway and W. G. Scanlon, "Antennas for over-body-surface communication at 2.45 GHz," *IEEE Trans. Antennas Propag.*, vol. 57, no. 4, pp. 844–855, Apr. 2009.

[8] W. Su, J. Zhu, H. Liao, and M. M. Tentzeris, "Wearable antennas for cross-body communication and human activity recognition," *IEEE Access*, vol. 8, pp. 58575–58584, 2020.

[9] C. Gabriel, "Compilation of the dielectric properties of body tissues at RF and microwave frequencies," Dept. Phys., King's Coll. London, London, U.K., Rep. TR-1996-0037, 1996.

[10] T. Kumpuniemi, M. Hämäläinen, K. Y. Yazdandoost, and J. Iinatti, "Human body shadowing effect on dynamic UWB on-body radio channels," *IEEE Antennas Wireless Propag. Lett.*, vol. 16, pp. 1871–1874, 2017.

[11] G. Lee, B. Garner, and Y. Li, "Simulation and measurement of electromagnetic wave propagation on dynamic human bodies," *IET Microw. Antennas Propag.*, vol. 11, no. 10, pp. 1347–1353, 2017.

[12] S. Obayashi and J. Zander, "A body-shadowing model for indoor radio communication environments," *IEEE Trans. Antennas Propag.*, vol. 46, no. 6, pp. 920–927, Jun. 1998.

[13] O. Landron, M. J. Feuerstein, and T. S. Rappaport, "A comparison of theoretical and empirical reflection coefficients for typical exterior wall surfaces in a mobile radio environment," *IEEE Trans. Antennas Propag.*, vol. 44, no. 3, pp. 341–351, Mar. 1996.

[14] J. Ryckaert, P. De Doncker, R. Meys, A. de Le Hoye, and S. Donnay, "Channel model for wireless communication around human body," *Electron. Lett.*, vol. 40, no. 9, pp. 543–544, 2004.

[15] L. Akhoondzadeh-Asl, Y. Nechayev, and P. Hall, "Surface and creeping waves excitation by body-worn antennas," in *Proc. Loughborough Antennas Propag. Conf.*, 2010, pp. 48–51.

[16] K.-K. Wong, K.-F. Tong, Z. Chu, and Y. Zhang, "A vision to smart radio environment: Surface wave communication superhighways," *IEEE Wireless Commun.*, vol. 28, no. 1, pp. 112–119, Feb. 2021.

[17] L. Akhoondzadeh-Asl, P. Hall, and Y. Nechayev, "Wave excitation on human body by a short dipole," in *Proc. 4th Eur. Conf. Antennas Propag.*, 2010, pp. 1–5.

[18] B. Ivsic, D. Bonefacic, Z. Sipus, and J. Bartolic, "An insight into creeping electromagnetic waves around the human body," *Wireless Commun. Mobile Comput.*, vol. 2017, Dec. 2017, Art. no. 2510196.

[19] D. U. Agu et al., "Investigation of dominant wave mechanism and optimal antenna excitation for body-centric wireless propagations," *Prog. Electromagn. Res. C*, vol. 104, pp. 1–11, Jul. 2020.

[20] J. Zhu and G. V. Eleftheriades, "A compact transmission-line metamaterial antenna with extended bandwidth," *IEEE Antennas Wireless Propag. Lett.*, vol. 8, pp. 295–298, 2009.

[21] N. P. B. Kammersgaard, S. H. Kvist, J. Thaysen, and K. B. Jakobsen, "Ear-to-ear propagation model based on geometrical theory of diffraction," *IEEE Trans. Antennas Propag.*, vol. 67, no. 2, pp. 1153–1160, Feb. 2019.

WENJING SU (Member, IEEE) received the B.S. degree in electrical engineering from the Beijing Institute of Technology, Beijing, China, in 2013, and the Ph.D. degree in electrical and computer engineering from the Georgia Institute of Technology, Atlanta, GA, USA, in 2018.

From 2013 to 2018, she was with the Agile Technologies for High-Performance Electromagnetic Novel Applications Research Group, led by Prof. M. M. Tentzeris. She was a Senior Hardware Engineer with Google LLC, Mountain View, CA, USA, from 2018 to 2021. She is currently an Antenna Research Scientist with Meta Platforms Inc. (formerly, known as Facebook Inc.), Sunnyvale, CA, USA. She has been the Lead Designer for several successfully shipped consumer hardware products in the market as well as the Lead Investigator for several new technology interception projects. She has authored/coauthored over 50 publications in refereed journals and conference proceedings and U.S. patents. Her research there interfaces advance novel fabrication techniques (e.g., inkjet-printing and 3-D printing), special mechanical structures (e.g., microfluidics and origami), and microwave components/antennas to solve problems in smart health, wearable electronics in the Internet of Things applications. Her research interests include wearable antennas, flexible electronics, on-body communication, additively manufactured electronics, wireless sensing, machine-learning aid sensing, green electronics, RFID, reconfigurable antennas, and anything for consumer hardware industry.

Dr. Su has been an Associate Editor for the IEEE TRANSACTIONS ON ANTENNAS AND PROPAGATION and a Reviewer for many IEEE publications, including PROCEEDINGS OF THE IEEE, *IEEE Antennas and Propagation Magazine*, IEEE TRANSACTIONS ON INDUSTRIAL ELECTRONICS, and IEEE TRANSACTIONS ON MICROWAVE THEORY AND TECHNIQUES. She has chaired many sessions in the IEEE conference and was the Track Chair of 2022 IEEE AP-S International Symposium on Antennas and Propagation and a TPC Member of 2019 IEEE MTT-S International Microwave Symposium and 2020 IEEE MTT-S Texas Symposium on Wireless Circuits and Systems.

PRATHAP VALALE PRASANNAKUMAR (Member, IEEE) received the M.S. and Ph.D. degrees in electrical engineering from the University of Colorado, Boulder.

Previously, he has worked as a Deputy Engineer with Bharat Electronics, India. He is an Antenna Engineer with the Reality Labs, Meta Platforms Inc. He has designed Oculus Quest 2 and Quest Pro antennas. His current research is focused on Wi-Fi (2.4, 5, and 6 GHz), Bluetooth, and UWB antennas and improving the isolation between collocated antennas in AR/VR consumer electronics devices. His Ph.D. thesis encompasses the design of monostatic, quasi-monostatic, and bistatic simultaneous transmit and receiver or in-band full-duplex antenna systems and wideband isolation enhancement techniques. His research interests include transmit and receive systems, broadband antennas, aperture antennas, high-impedance surfaces, reflector antennas, and computational electromagnetic.

Dr. Prasannakumar received the Raska Mantri's Award from the Ministry of Defense, Government of India, during his tenure in Bharat Electronics Ltd.

YIXIANG LI received the B.S. and M.S. degrees in electrical engineering from Tsinghua University, Beijing, China, in 1999. From 2004 to 2014, he was a Senior Staff Engineering Manager with Qualcomm, San Jose, CA, USA, managing a team of talents driving Wi-Fi silicon system-level performance tuning and improvement, including Qualcomm's 1st Gigabit Wireless Router featuring 3 × 3 802.11ac and Qualcomm's most advanced Wi-Fi for mobile 2 × 2 802.11ac. From 2014 to 2021, he was a Senior Hardware Engineer with Google Inc., Mountain View, CA, USA, leading Wi-Fi mesh/AP performance efforts in launching Google's first generation and next generation of Wi-Fi home router products. In 2021, he joined Meta Reality Labs, Sunnyvale, CA, USA, as the Wireless Platform Manager, leading a team of talents in developing next generation of Wi-Fi performance for the VR/AR products.

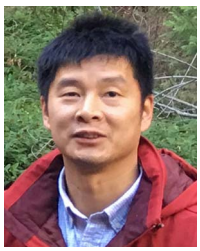

GENG YE is the Head of Antenna Engineering with Meta Reality Labs, Sunnyvale, CA, USA. He has been instrumental in creating unique antenna designs for Meta's virtual/artificial reality devices.

JIANG ZHU (Fellow, IEEE) received the B.S. degree in information science and electronic engineering from Zhejiang University, China, the M.A.Sc. degree in electrical engineering from McMaster University, Canada, and the Ph.D. degree in electrical engineering from the University of Toronto, Canada.

From 2010 to 2014, he was a Senior Hardware Engineer with Apple Inc., Cupertino, CA, USA. From 2014 to 2016, he was with Google[x] Life Science Division and then a Founding Member with Verily Life Science, a Subsidiary of Alphabet Inc., Mountain View, CA, USA. From 2016 to 2021, he founded the Wearable Wireless Hardware Group, at Google LLC, Mountain View, and led the antenna and RF research and development for the emerging wrist-worn, hearable, virtual reality and augmented reality products, projects, and technologies. In 2021, he joined Meta Reality Labs, Sunnyvale, CA, USA, as the Head of Antenna Research, where he leads a group of talented and diverse research scientists and engineers working on the enabling technologies for the immersive wearable computing. His work leads to over 100 IEEE journal and conference publications and U.S. patents, many of them have been commercialized in some of the most popular consumer products in the world. His research interests are the consumer applications of RF, antennas, and electromagnetics in the areas of wireless communications, human body interaction and sensing, and wireless power.

Dr. Zhu was a recipient of the IEEE Microwave Theory and Techniques Society Outstanding Young Engineer Award and the IEEE Antennas and Propagation Society Doctoral Research Award. He has received several Student Paper Awards as a student as well as a Project Supervisor, including the most recent one—the First Place Best Student Paper Award in the 2021 IEEE AP-S Symposium on Antennas and Propagation with his intern student at Google. He has been a Senior Editor for the IEEE OPEN JOURNAL OF ANTENNAS AND PROPAGATION and an Associate Editor for the IEEE TRANSACTIONS ON ANTENNAS AND PROPAGATION, the IEEE INTERNET OF THINGS JOURNAL, the IEEE ANTENNAS AND WIRELESS PROPAGATION LETTERS, and *IET Microwaves, Antennas, and Propagation*. He is also the Guest Co-Editor for the *IEEE Communications Magazine*—Special Feature Topic on Antenna Systems for 5G and Beyond, and the IEEE OPEN JOURNAL OF ANTENNAS AND PROPAGATION—Special Section on Advances in Antenna Design for Metaverse and Other Modern Smart Mobile Devices. He is a member of the IEEE AP-S Industrial Initiatives Committee and the IEEE AP-S Young Professional Committee, a member and the Industry Liaison of the IEEE AP-S Membership and Benefits Committee, and a member of the IEEE MTT-S Technical Coordination Future Directions Committee—IoT Working Group, the IEEE MTT-26 RFID, Wireless Sensors, and IoT Committee. He serves as the TPC Chair for the 2023 IEEE International Workshop on Antenna Technology, and the TPC Co-Chair for the 2022 IEEE International Microwave Biomedical Conference. He serves on TPC and TPRC for numerous conferences, including IEEE APS, IMS, and RWS.